

Optical properties of strontium doped BaTiO₃ thin films by thermal evaporation method for optoelectronic devices

R. SENGODAN^{a,*}, B. CHANDRA SHEKAR^{b,*}

^aDepartment of Physics, Kumaraguru College of Technology, Coimbatore – 641049, Tamil Nadu, India

^bDepartment of Physics, Kongunadu Arts and Science College, G.N- Mills, Coimbatore – 641029, Tamil Nadu, India

In the present work, the prepared nano powders were thermally grown onto well cleaned glass substrates under the vacuum of 10⁻⁵ torr, using 12A4 Hind Hivac coating unit. The X-ray diffraction patterns shown that Sr doped BaTiO₃ nanoparticles possess tetragonal structure and the deposited films were polycrystalline in nature. Absorption coefficient, extinction coefficient, optical band gap and refractive index of films were estimated from optical transmittance spectrum. The extinction coefficient of films decreases with increase in thickness and refractive index of the films increases with increase in thickness. The optical band gap energy value varies from 3.90eV to 3.75eV with increase of thickness.

(Received September 1, 2019; accepted June 16, 2020)

Keywords: Sr doped BaTiO₃, Thermal evaporation, UV-Visible

1. Introduction

Ferroelectric thin films have found wide applications in many electronic and electro-optic devices [1]. Among these, Sr doped BaTiO₃ titanate is currently one of the most interesting ferroelectric materials due to its high dielectric permittivity, low optical losses and composition dependent Curie temperatures. The Sr doped BaTiO₃ thin films are also attractive candidates for non-linear optical devices such as planar wave guides, optical modulators, optical windows, optical switches, optical filters etc. with minimal optical propagation losses. Sr doped BaTiO₃ thin films have been deposited by several methods sol-gel method [2, 3], chemical solution deposition [4], pulsed laser ablation [5] and radio-frequency (rf) sputtering [6]. Among the various methods, vacuum evaporation is an excellent method to produce thin films on various substrates with good stoichiometry that can easily be up scaled for industrial applications. Properties of thin films are dependent on various deposition parameters like deposition technique, thickness, total pressure and composition of the operating gas. The thickness plays a pivotal role in Sr doped BaTiO₃ thin film properties like orientation, crystallinity and surface morphology [7]. The function of Sr doped BaTiO₃ thin films in opto-electronic devices depends on structural and optical properties like grain size, lattice distortion, micro-strain, band gap, refractive index and absorption. It is important to study how these properties depend on deposition parameters. Several studies suggest that a strong correlation between the optical properties and the crystalline structure of the perovskite thin films exists. The band gap is the best example: with increasing crystallinity of the films the band gap decreases [8]. In this paper, we investigate Sr doped BaTiO₃ thin films prepared by vacuum evaporation and study their structural and optical properties and their surface morphology at various thickness

2. Experimental details

2.1. Synthesis of Strontium (Sr) doped BaTiO₃ nanoparticles

Sr doped BaTiO₃ nanoparticles were synthesized by using wet chemical method. The starting materials used were barium chloride (BaCl₂·2H₂O, Aldrich Chemicals, purity 98%), titanium dioxide (TiO₂, Merck chemicals, purity 99%), strontium carbonate (SrCO₃, Merck chemicals, purity 99%) powder and oxalic acid (Merck chemicals, purity 99%). A solution of Ba: Ti: oxalic acid: SrCO₃ having mole ratio 1:1: 1: 0.1 was stirred and evaporated at 70 °C till a clear, viscous resin was obtained and then dried at 110 °C for 20h. The precursor formed was calcined at 900 °C for 2h using muffle furnace to form Sr doped BaTiO₃ nanoparticles.

2.2. Sr doped BaTiO₃ thin film preparation

The prepared nanopowders of Sr doped BaTiO₃ placed in the molybdenum boat (200 amps) and get heated with high current by energizing transformer. The transformer capable of supplying 150 amperes at 20 volts is used to provide the necessary current for heating the molybdenum source. Prior to evaporation, the evaporated material was carefully degassed at a lower temperature for about thirty minutes with the shutter closed. Deposition of the material on to pre-cleaned glass substrates under the pressure of about 10⁻⁵ Torr was achieved by slowly varying the current. A constant rate of evaporation 1Å/sec was maintained throughout the film preparation. The adhesion of the films to the substrate seems to be extremely good. The substrate to source distance was optimized to be at 0.175 m and source to crystal distance was optimized to be at 0.21 m inside the vacuum chamber. The deposited thin films of

various thickness were used to study the structure, morphology and optical properties.

2.3. Measurements

Thickness of the films was measured through quartz crystal monitor ("Hind Hivac" Digital Thickness Monitor Model-DTM-101). The structural aspects of the films were analyzed, using X-ray diffractometer with filtered CuK α radiation ($\lambda = 1.5418 \text{ \AA}$). The surface morphology of the films was examined by scanning electron microscope (SEM) and the high-resolution transmission electron microscopy (HRTEM). The optical studies were carried out by using JASCO – UV/VISIBLE spectrophotometer (JASCO V – 670, Japan).

3. Result and discussion

3.1. Scanning Electron Microscope (SEM)

Studies

Fig. 1 shows the SEM images of Sr doped BaTiO₃ nanoparticles. Surface morphology of the nanoparticles revealed the presence of spherical and rod like grain structure distributed throughout the particles. Figure 2 (a, b, c) shows the SEM images of the Sr doped BaTiO₃ thin films at different thickness. The grain size of these films are lower than the grain size of pure BaTiO₃ thin films, which is due to doping of Sr in BaTiO₃. In all the films micro cracks were observed. These are attributed to the volume contraction during the crystallization process and the stress caused by the mismatch in thermal expansion coefficient between the film and substrate [9]. The grain size of the films increases with increasing thickness, it could be attributed to higher grain growth at higher thickness [10].

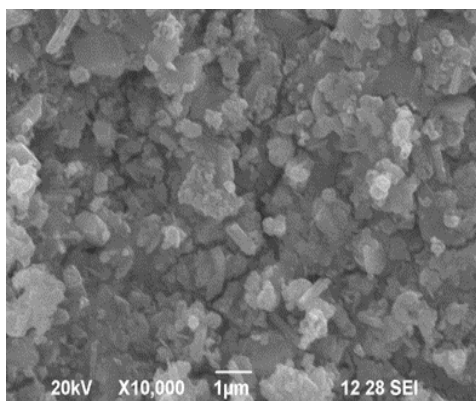


Fig. 1. SEM images of Sr doped BaTiO₃ nanoparticles

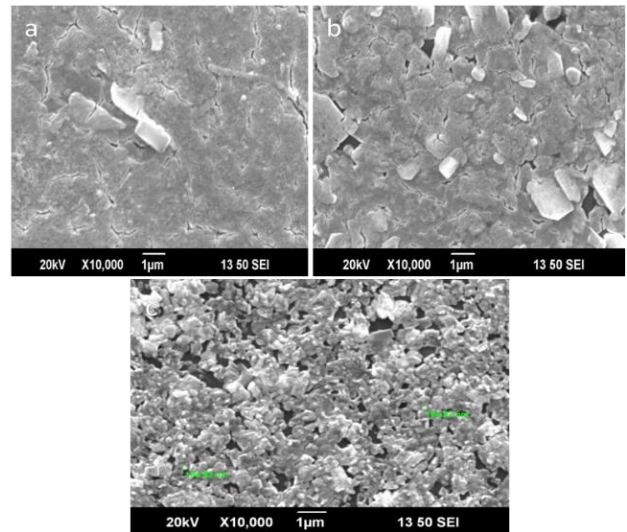


Fig. 2. SEM images of Sr doped BaTiO₃ thin films of thickness (a) 80nm (b) 150nm (c) 165nm (color online)

3.2. Transmission Electron Microscope

Fig. 3 shows the HRTEM micrograph of the Sr doped BaTiO₃ nanoparticles with a well -isolated rod like morphology. The diameter of the rod is less than 100 nm.

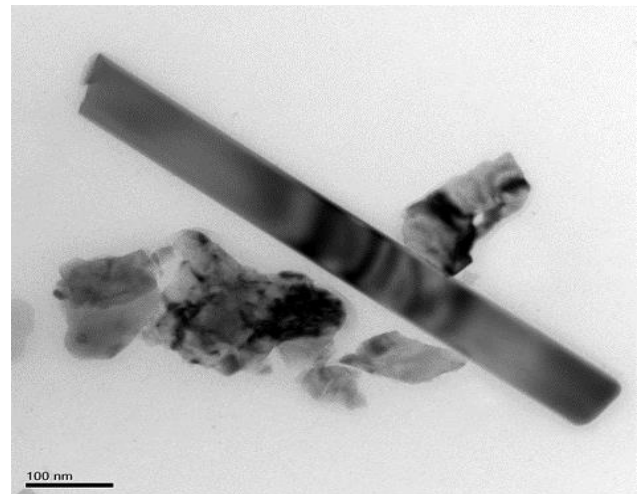


Fig. 3. HRTEM micrograph of Sr doped BaTiO₃

3.3. X – Ray Diffraction Analysis

Fig. 4 shows the XRD pattern of Sr doped BaTiO₃ nanoparticles calcined at 900 °C temperature for 2h. The peak splitting observed at an angle of $2\theta = 44^\circ$ to 46° indicated tetragonal structure. As the Sr is doped with BaTiO₃, the crystallinity of the material increases whereas the diffraction peaks shift towards higher angles as compared with the undoped BaTiO₃ nanoparticles [11]. This may be due to the decreased interatomic spacing and variation of lattice parameters by doping Sr with BaTiO₃ nanoparticles [12, 13]. This effect can be explained by the fact that the ionic radius of Sr²⁺ (0.113 nm) is smaller than the ionic radius of Ba²⁺ (0.135 nm) [14, 15].

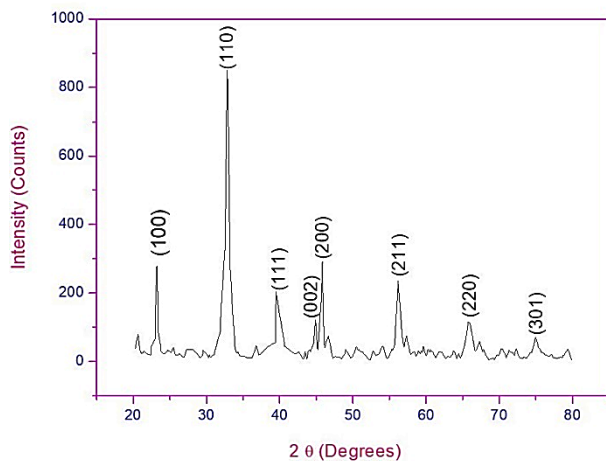


Fig. 4. XRD pattern of Sr doped BaTiO₃ nanoparticles (color online)

The crystallite size is calculated from the Scherrer's formula from the full width at half – maximum (FWHM) of the XRD peaks

$$D = 0.94\lambda / \beta \cos\theta \quad (1)$$

where λ is the wavelength of the X-rays used, 2θ is the angle between the incident and scattered X-rays and β is the full width at half maximum. The strain (ϵ) is calculated from the formula

$$\epsilon = \beta \cos\theta / 4 \quad (2)$$

The dislocation density (δ) is defined as the length of dislocation lines per unit volume of the crystal and is given by

$$\delta = 1/D^2 \quad (3)$$

The crystallite size was calculated at different diffraction angles and tabulated in the Table 1. From the Table it is observed that crystallite size varies between 33 nm to 45 nm.

Table 1. Structural parameter of Sr doped BaTiO₃ nanoparticles

Temperature (°C)	Calculated values			Crystallite size (nm)
	2θ (Degrees)	d (Å)	h k l	
900	23.67	3.7	100	36.45
	32.84	2.5	110	45.38
	39.67	2.2	111	35.43
	46.08	1.9	002	33.78
	56.057	1.6	211	42.53
	66.426	1.4	220	42.56
	74.95	1.2	301	43.34

3.4. Effect of thickness on Sr doped BaTiO₃ thin films

Fig. 5 shows the XRD patterns of the Sr doped BaTiO₃ thin films of different thickness deposited on glass substrate. It shows that the films of lower thickness (80 nm) showed amorphous nature. As the thickness increases (>80 nm) the films showed polycrystalline nature. The orientation of the peaks were found to be (001) (110), (111), (200), (102) and (112) corresponding to 2θ values of 23.95°, 30.30°, 36.84°, 43.06°, 52.64° and 56.63° respectively. The intensity of the peak corresponding to (110) orientation was found to be higher than the peaks corresponding to the (111) and (200) orientation. As can be seen, the crystallization of the films strongly depends on the film thickness. The intensity of the peak increases with increase in film thickness, indicating good crystallinity. However, it is seen that for 165 nm thickness of the film distinct splitting of the (200/002) peaks are evident indicating tetragonal structure [16]. In all the Sr doped BaTiO₃ thin films the diffraction peaks shift towards higher angles when compared to pure BaTiO₃ thin films [17], which is indicative of a decrease in the lattice constant, interatomic spacing and change in interplanar distance of the films [18]. This lattice shrinkage is due to the substitution of smaller size Sr²⁺ ions (0.113 nm) in the lattice of the larger size Ba²⁺ ions ($r = 0.135$ nm).

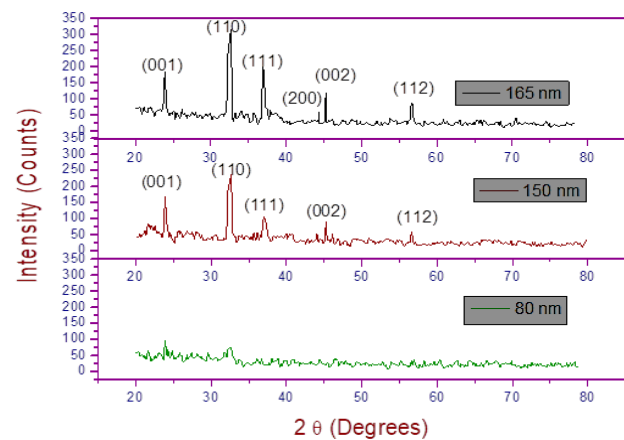


Fig. 5. XRD pattern of Sr doped BaTiO₃ films of different thickness (color online)

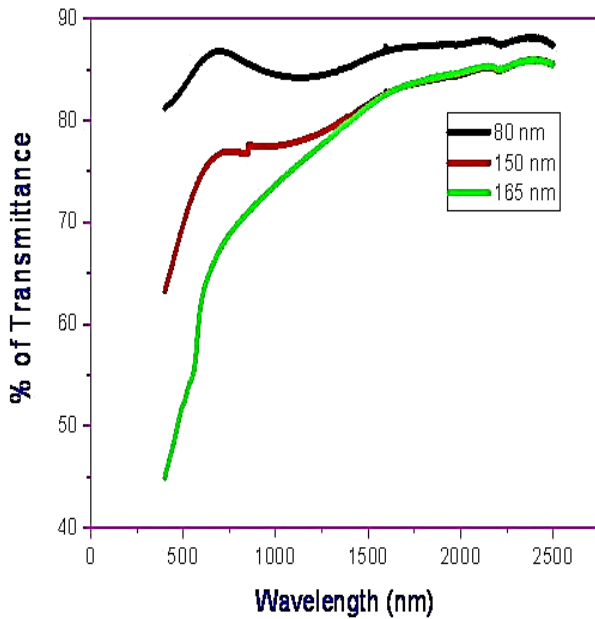
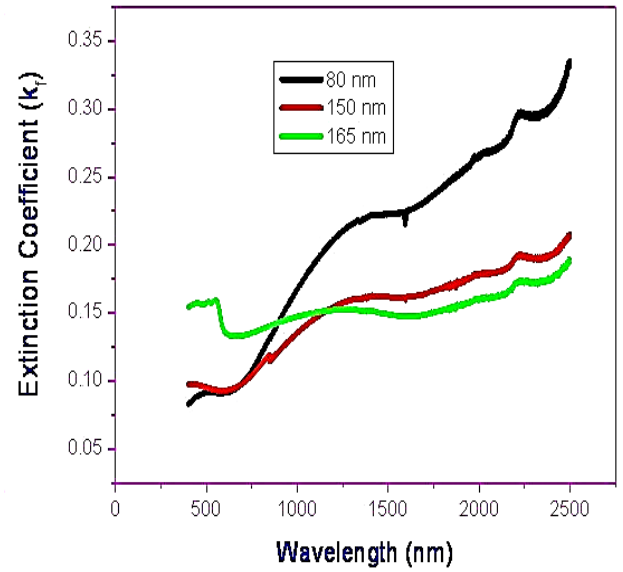
The crystallite size (D), dislocation density (δ) and strain (ϵ) for different thickness as shown in the table 2. From this Table, an appreciable decrease in crystallite size is observed when compared to the pure BaTiO₃ films. The decrease in crystallite size with Sr doped BaTiO₃ thin films may be due difference in size between the Ba²⁺ and Sr²⁺ of barium composition. It is also observed that the crystallite size increases with increase of film thickness whereas the strain and the dislocation density decrease with increase of film thickness.

Table 2. Structural parameters of Sr doped BaTiO₃ thin films of different thickness

Thickness (nm)	2θ Degrees	hkl	Crystallite size(D) (nm)	Strain (ε) x10 ⁻³ (lin ⁻² m ⁴)	Dislocation density (δ) X10 ¹⁵ (lin/m ²)
150	24.08	100	24.28	1.427	1.696
	32.66	110	26.23	1.320	1.453
	39.01	111	21.25	1.631	2.214
	45.14	002	20.31	1.706	2.426
	56.61	112	23.62	1.467	1.792
165	24.08	100	25.86	1.340	1.495
	32.66	110	28.45	1.218	1.235
	39.01	111	23.13	1.498	1.869
	45.14	002	20.69	1.673	2.336
	56.61	112	24.87	1.393	1.616

3.5. Optical studies

The transmittance spectra of Sr doped BaTiO₃ thin film of different thicknesses is shown in figure 6. It is clearly observed that transmittance decreases with increasing in thickness [19]. It is also detected that these films have low transmittance when compared to the pure BaTiO₃ films [20]. This decrease in the transmission can be attributed to the introduction of impurity level between valance band and conduction band [21, 22]. The transmittance in the higher wavelength range is less than that of pure BaTiO₃ films. This may be due to the fact that Sr doped BaTiO₃ films had higher carrier concentration than pure BaTiO₃ films, as absorption in the near-infrared region is mainly due to free carriers.

Fig. 6. Transmittance spectra of Sr doped BaTiO₃ films of different thicknesses (color online)Fig. 7. Extinction coefficient of Sr doped BaTiO₃ films of different thicknesses (color online)

In order to describe the fundamental absorption edge, the spectral dependence of absorption coefficient (α) is directly determined using the relation,

$$\alpha = \frac{4\pi k_f}{\lambda} \quad (4)$$

where λ is the wavelength of the incident radiation and k_f is the extinction coefficient.

The extinction coefficient is defined as,

$$k_f = \frac{2.303 \log_{10} \left(\frac{1}{T} \right) \lambda}{4\pi t} \quad (5)$$

where 't' is film thickness. The nature of transition can be investigated on the basis of dependence of α on the photon energy $h\nu$. For direct and allowed transitions, the theory of fundamental absorption leads to the following photon energy dependence near the absorption edge as,

$$\alpha \propto [h\nu - E_g]^m \quad (6)$$

where $h\nu$ and E_g are the photon energy and the optical energy gap respectively. In this expression, the values of m are 1/2 and 2 for direct and indirect transition respectively.

The optical properties of any material are characterized by two parameters n and k_f . The plot of transmission T against wavelength λ is found to vary as [17]

$$T = \frac{16n_a n_g n^2 \exp(-\alpha t)}{R_1^2 + R_2^2 \exp(-2\alpha t) + 2R_1 R_2 \exp(-\alpha t) \cos(4\pi t/\lambda)} \quad (7)$$

where

$$R_1 = (n + n_a)(n_g + n)$$

$$R_2 = (n - n_a)(n_g - n)$$

α is the absorption coefficient and n, n_a, n_g are the refractive indices of the film, air and substrate respectively. Iterations were carried out till the desired convergence was achieved.

The porosity (ρ) values (Volume of pores per volume of film) of the films were calculated using the relation [18]

$$\rho = 1 - \frac{n_f^2 - 1}{n_b^2 - 1} \times 100 \quad (8)$$

Fig. 7 shows the variation of extinction coefficient with wavelength for Sr doped BaTiO₃ thin films of different thickness. It is observed that extinction coefficient decreases with increase in thickness. It is also noted that the extinction coefficient value of the Sr doped BaTiO₃ film lightly decreases when compared to pure BaTiO₃ thin films [20].

Fig. 8 shows the variation of absorption coefficient (α) with wavelength of Sr doped BaTiO₃ thin films of different thickness. From the absorption coefficient (α) the band gap

energy of the films were calculated by using the equation (6).

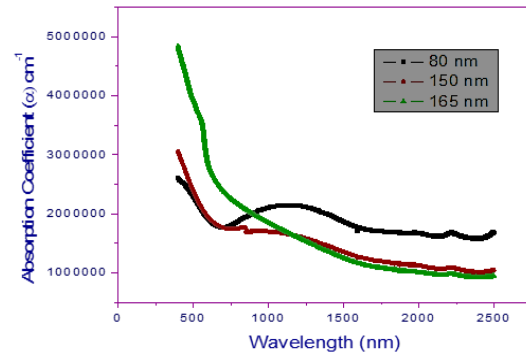


Fig. 8. Variation of absorption coefficient (α) with wavelength of Sr doped BaTiO₃ thin films of different thickness (color online)

Fig. 9 shows the variation of $(\alpha h\nu)^2$ versus photon energy for Sr doped BaTiO₃ thin film of different thickness, indicating the possible optical transition is of direct-allowed type and the band gap energies are given in table 3. It is observed that band gap of the film decreases with increases of thickness [23]. The appreciable decrease in the band gap of Sr doped BaTiO₃ films may also be caused by the presence of internal electric fields associated with the defects and by the changes in composition of the films.

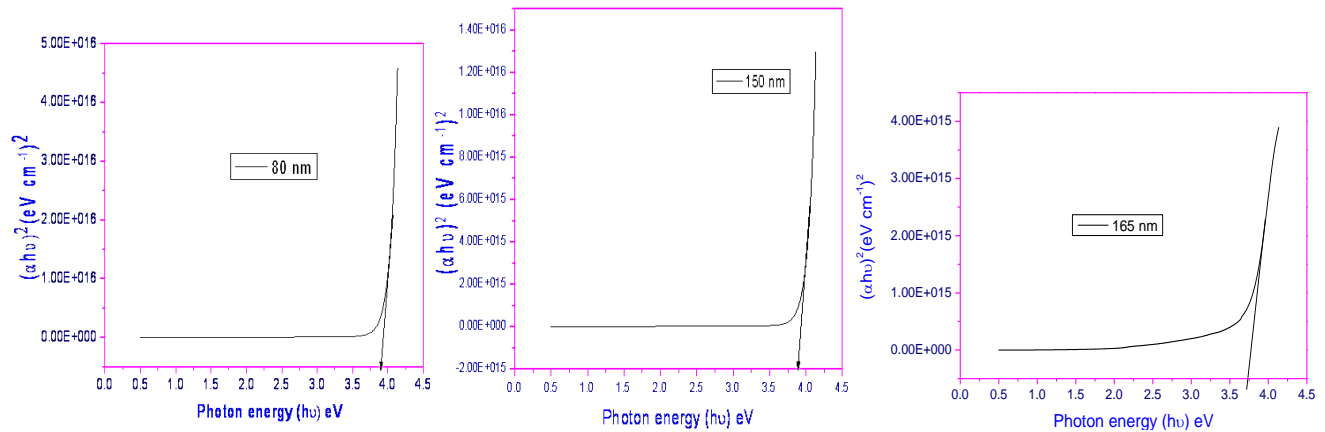


Fig. 9. Plot $(\alpha h\nu)^2$ vs $h\nu$ for Sr doped BaTiO₃ films of various thicknesses (color online)

Table 3. Band gap energy of Sr doped BaTiO₃ film of thickness 150 nm at different annealing temperatures

Thickness (nm)	Band gap energy (eV)
80	3.90
150	3.87
165	3.75

Table 4 shows the porosity of the Sr doped BaTiO₃ thin film of different thickness. It is observed that porosity decreases with increase in thickness.

Table 4. Porosity of the Sr doped BaTiO₃ thin film of thickness 165 nm annealed at different temperatures

Thickness (nm)	Porosity (ρ) %
80	49.6
150	40
165	38.80

Fig. 10 shows the refractive index with wavelength for Sr doped BaTiO₃ thin films of different thickness. It is seen that refractive index increases with increasing thickness. The refractive index of the Sr doped BaTiO₃ thin films are

high compared to pure BaTiO₃ thin films. It is due to decrease in porosity of the Sr doped BaTiO₃ thin films.

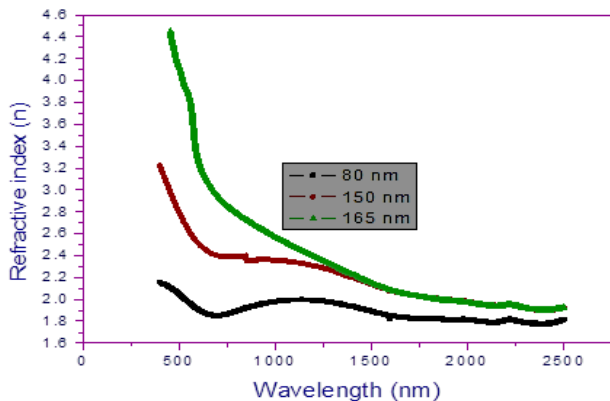


Fig. 10. Variation of refractive index with wavelength for Sr doped BaTiO₃ thin films of thickness 165 nm for different annealing temperatures (color online)

4. Conclusion

Sr doped BaTiO₃ nanopowders were successfully prepared by wet chemical method. The prepared nanopowders were thermally deposited onto well cleaned glass substrates by thermal evaporation method. X-ray analysis of prepared nanoparticles showed that particle has a tetragonal nature and the deposited film has a polycrystalline nature. From the transmission spectra, the transmittance is found dependent on the thickness. The transmittance decreases with increase in thickness. The value of extinction coefficient decreases with increases in thickness. The refractive index of the films increases with increase in thickness. The possible optical transition is direct-allowed type. The optical band gap energy shows an inverse dependence thickness.

References

- [1] S. Bobby singh, H. B. Sharma, H. N. K. Sarma, Sumitra Phanjoubam, *Modern Physics Letters B* **22**, 693 (2008).
- [2] H. B. Sharma, A. Mansingh, *J. Phys. D: Appl. Phys.* **311**, 527 (1998).
- [3] Z. Hu, G. Wang, Z. Huang, X. Meng, J. Chu, *Semicond. Sci. Technol.* **18**, 449 (2003).
- [4] J. Petzelt, T. Ostapchuk, A. Paskin, I. Rychetsky, *J. Eur. Ceram. Soc.* **23**, 2627 (2003).
- [5] P. Bhattacharya, T. Komeda, D. Park, Y. Nishioka, *J. Appl. Phys.* **32**, 4103 (1993).
- [6] Q. X. Jia, J. L. Smith, L. H. Chang, W. A. Anderson, *Phil. Mag. B* **77**, 163 (1998).
- [7] J. Zhang, D. Cui, H. Lu, Z. Chen, Y. Zhou, L. Li, *Japan. J. Appl. Phys.* **36**, 276 (1997).
- [8] M. N. Kamalasanan, N. D. Kumar, S. Chandra, *J. Appl. Phys.* **76**, 4603 (1994).
- [9] C. B. Samantaray, A. Dhar, D. Bhattacharya, M. L. Mukherjee, S. K. Ray, *J. Mater. Sci.: Mater. Electron.* **12**, 365 (2001).
- [10] M. Melo, E. B. Araujo, V. V. Shvartsman, V. Ya. Shur and A. L. Kholkin, *Journal of applied physics* **120**, 054101 (2016).
- [11] R. Sengodan B. Chandar Shekar, R. Balamurugan, R. Kannan, R. Ranjithkumar, *J. Optoelectron. Adv. M.* **19**, 595 (2017).
- [12] V. Somani, S. M. Kalita, *J. Electroceram.* **18**, 57 (2007).
- [13] A. Wu, P. M. Vilarinho, M. Gonzalez, *J. Nanopart. Res.* **12**, 2221 (2010).
- [14] A. J. Moulson, J. M. Herbert, *Electroceramics: Materials, Properties and Applications*, 2nd edition, Wiley, New York (2003).
- [15] J. Ravez, A. Simon, *J. Solid State Chemistry.* **162**, 260 (2001).
- [16] Z. Hu, G. Wang, Z. Huang, X. Meng, Q. Zhao, J. Chu, *Appl. Phys. A* **78**, 757 (2004).
- [17] Raja Sengodan, Bellan Chandar Shekar, Sugumaran Sathish, *Optik* **125**, 4819 (2014).
- [18] H. Chen, C. Yang, J. Zhang, W. Leg, H. Ji, Z. Wang, J. Liao, L. Zhano, *J. Mater. Sci.: Mater. Electron.* **21**, 236 (2010).
- [19] Sengodan Raja, Gopal Subramani, Dinesh Bheeman, Ranjithkumar Rajamani, Chandar Shekar Bellan, *Optik* **127**, 461 (2016).
- [20] Sengodan, B. Chandar Shekar, S. Sathish *J. Optoelectron. Adv. M.* **14**, 653 (2012).
- [21] D. K. Schroder, *Semiconductor Material Device Characterization*, 2nd edn., Wiley, New York, 1998.
- [22] R. M. Rose, L. A. Shepard, J. Wulff, *The Structure and Properties of Materials*, Vol. 4, John Wiley and Sons Inc., New York, 1967.
- [23] R. P. Khatri, S. M. Vyas, Dimple Shah, Piyush Patel, M. P. Jani, G. R. Pandya, *International Journal of Physics and Applications* **2**, 95 (2010).

*Corresponding authors: chandar.bellan@gmail.com
sengodan78@gmail.com